



Dissipatively stabilized superposition of squeezed coherent states via periodically breaking the qubit inversion symmetry

Peng Xie,¹ Xing-chen Wang,¹ Jing-wei Wang,¹ Xin-ke Li ,^{1,*} Yuan Zhou,^{1,2} Guang-hui Wang,³
Fazal Badshah ,² and Yong-chen Xiong¹

¹*School of Mathematics, Physics and Optoelectronic Engineering, Shiyan Key Laboratory of Quantum Information and Precision Optics, Hubei Key Laboratory of Energy Storage and Power Battery, and Collaborative Innovation Center for Optoelectronic Technology, Hubei University of Automotive Technology, Shiyan 442002, China*

²*School of Electrical and Information Engineering, Hubei University of Automotive Technology, Shiyan 442002, China*

³*School of Automobile Engineering, Hubei University of Automotive Technology, Shiyan 442002, China*



(Received 21 September 2023; revised 2 March 2024; accepted 16 April 2024; published 7 May 2024)

We propose a scheme to dissipatively stabilize superpositions of squeezed coherent states for single- and two-resonator modes in superconducting circuits, where a superconducting qubit is coupled to a single or two parametrically driven transmission-line resonators with different circuit designs. A modulated magnetic flux applied to the qubit can periodically break the inversion symmetry of the qubit and induce both the parametrically enhanced transverse and longitudinal couplings to the resonators, resulting in strong nonlinear two-photon interactions between the qubit and the resonators and enabling the scheme to be implemented in a relatively weak coupling regime. With an additional microwave drive applied to the qubit, the dissipation of the qubit used as a resource can help drive the resonators into the desired superpositions of squeezed coherent states at a steady state with high speed. Numerical simulations show that the target states with high fidelity and highly nonlinear properties can be created for a long time even in the presence of photon leakage out of the resonators. The scheme can be generalized to other quantum platforms and may have potential applications in the field of quantum information processing and the improvement of estimation precision in quantum metrology.

DOI: [10.1103/PhysRevA.109.052409](https://doi.org/10.1103/PhysRevA.109.052409)

I. INTRODUCTION

Multiphoton entangled states are essential resources and denote a key prerequisite for many applications in quantum information science [1,2]. Of particular interest are the superpositions of coherent states [3]. As nonlocal quantum superpositions confined in phase space, such states play a key role in fundamental tests of quantum theory in macroscopic systems [4–6] and high-precision measurements surpassing the quantum-noise limit [1,7]. Especially, the superpositions of coherent states can be used to encode logical qubits, allowing for exponential suppression of bit flips and protection against photon dephasing errors and single-photon loss, forming an ideal building block for scalable fault-tolerant quantum computation with a significant reduction in hardware overhead [8–12]. For superpositions of squeezed coherent states, the introduction of squeezing can further improve the protection against decoherence [13,14], while at the same time enabling us to partially correct errors caused by photon loss [15]. Such states can be generated by N -phonon detection or homodyne detection based on preprepared multiphoton states as resources [13,16,17] or by introducing additional Josephson junction devices or quadratic optomechanical coupling to induce two-photon interaction between subsystems [18–20]. Recently, an all-optical scheme was proposed to

deterministically create superpositions of squeezed coherent states based on dissipation; however, three optical modes are needed to induce Fredkin-type interaction [21].

Symmetry breaking provides a promising route to quantum state manipulation [22–24]. It is ubiquitous in many fields of physics and plays a key role in many physical phenomena, especially in the presence of elementary particles described by quantum fields, quantum-mechanical descriptions of condensed-matter systems, and so on [25,26]. For natural atoms and molecules, their inversion symmetry can be broken by either a strong external field or absorption of a linearly polarized photon [27,28], while the breaking of the inversion symmetry for artificial atoms can be controlled by tuning externally applied parameters [29–31]. For instance, when the superconducting flux qubit and charge qubit are operated away from their degeneracy point by tuning bias charge and bias magnetic fluxes, respectively, the inversion symmetry of their potential energies can be broken. In this case, the selection rule breaks down, and microwave-photon transitions between any two energy levels are possible, leading to an additional longitudinal coupling to radiation fields and allowing for new methods for the manipulation of quantum states, multiphoton bundle emission, and engineering of universal multiqubit architecture [22–24,32–36]. In general, superconducting qubits with broken inversion symmetry suffer from more susceptibility to offset charge noise or flux noise and shorter coherence times. However, a recent development in the optimization of the superconducting-qubit design allows for

*20210064@huat.edu.cn

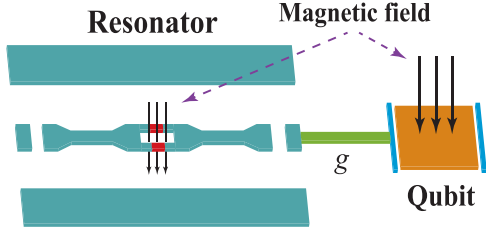


FIG. 1. Schematic diagram of a TLR coupled to a superconducting qubit. The central line of the TLR is intersected by a SQUID loop, which can induce a parametric drive on the TLR when an external magnetic field is applied. The red segments in the superconducting lines denote Josephson junctions.

both long coherence times and large anharmonicity [37–40], providing new possibilities for the further application of qubit inversion-symmetry breaking.

In this work, an efficient scheme is presented for the creation of long-lived superpositions of squeezed coherent states in superconducting circuits via periodically breaking the qubit inversion symmetry. The setup consists of a superconducting qubit coupled to a transmission-line resonator (TLR). The TLR is subjected to a parametric driving realized by tuning the magnetic flux penetrating the resonator-embedded superconducting quantum interference device (SQUID) loop, enabling great enhancement of the coupling strength between the qubit and the resonator and allowing for the implementation of the scheme in a relatively weak regime. The inversion symmetry of the qubit can be periodically broken by modulating the external magnetic field applied to the qubit, resulting in both transverse and longitudinal couplings of the qubit to the resonator. The induced nonlinear two-photon interaction is much stronger than that induced by the cross-Kerr effect and can be further enhanced by the parametric driving. In the case that the qubit is driven by an additional microwave field and is largely damped, the quantized field in the resonator will be driven into superpositions of squeezed coherent states at a steady state with high speed. Moreover, we extend our scheme to include an additional resonator and study the generation of superpositions of squeezed coherent states for two modes, where the circuit can be designed in two different ways. Fidelities and Wigner functions of the created states are calculated numerically, and the results show that the created states exhibit highly nonclassical properties and target states with high fidelity can be generated at steady state even in the case when the photon leakage of the resonators is considered. Compared with the results of previous works [13,16–20], the target states can be deterministically created without the preparation of certain initial states or additional quantum devices or quadratic optomechanical coupling to induce necessary nonlinear interaction.

II. GENERATION OF SUPERPOSITIONS OF SQUEEZED COHERENT STATES FOR A SINGLE MODE

A. Model

As shown in Fig. 1, the setup under consideration consists of a TLR coupled to a superconducting qubit. The TLR contains a narrow central conductor with two breaks acting as

capacitors and two ground planes placed on the two sides of the central line, keeping the resonator well isolated from its environment [41,42]. In the case that the TLR is modeled as a simple harmonic oscillator and only the fundamental mode is considered, its free Hamiltonian takes the form (hereafter $\hbar = 1$)

$$H_r = \omega_r a^\dagger a, \quad (1)$$

where ω_r is the resonance frequency of the resonator mode and a (a^\dagger) is the corresponding annihilation (creation) operator. When the resonator is embedded with a SQUID loop, an external magnetic field penetrating the loop can modify the eigenstates of the resonator and lead to a parametric driving of the resonator with the following form [43–46]:

$$H_p = -\frac{\lambda(t)}{2} (a^{\dagger 2} e^{-i\omega_p t} + a^2 e^{i\omega_p t}), \quad (2)$$

in which $\lambda(t)$ is the time-dependent two-photon driving amplitude and ω_p is the driving frequency. An amplified fluctuation of resonator photons can be induced by the parametric driving, resulting in exponentially enhanced effective qubit-resonator coupling [47,48].

The superconducting qubit could be a flux qubit or a fluxonium qubit, whose two lowest energy levels are well isolated from the upper levels [29–31]. When projecting the full Hamiltonian of the qubit onto the two lowest-energy states, i.e., the ground state $|\bar{g}\rangle$ and the excited state $|\bar{e}\rangle$, we can obtain the following reduced Hamiltonian [29,40]:

$$H_q = \frac{1}{2} \bar{\omega}_q \bar{\sigma}_z + \frac{1}{2} \bar{\varepsilon} \bar{\sigma}_x, \quad (3)$$

where $\bar{\sigma}_z = |\bar{e}\rangle\langle\bar{e}| - |\bar{g}\rangle\langle\bar{g}|$ and $\bar{\sigma}_x = \bar{\sigma}_+ + \bar{\sigma}_- = |\bar{e}\rangle\langle\bar{g}| + |\bar{g}\rangle\langle\bar{e}|$ are the Pauli operators and $\bar{\omega}_q$ and $\bar{\varepsilon}$ are the energy gap of the qubit and the magnetic energy bias, respectively. The magnetic energy bias $\bar{\varepsilon}$ is proportional to $(\Phi_{\text{ext}}^q - \Phi_0/2)$, with $\Phi_0 = h/2e$ being the flux quantum and Φ_{ext}^q being the external magnetic flux penetrating the qubit loop; thus, it can be tuned on demand by choosing appropriate external magnetic fields, allowing for the controllable breaking of the inversion symmetry of its energy potential.

The qubit can couple to the quantized microwave field of the resonator by connecting parallel and series circuits with wires or via a coupler such as a capacitance. The interaction Hamiltonian can be written as [37,49,50]

$$H_{\text{int}} = g(a\bar{\sigma}_+ + a^\dagger\bar{\sigma}_-), \quad (4)$$

where g is the coupling strength of the qubit to the resonator, describing the hopping of microwave photons between them.

B. Periodic breaking of the qubit inversion symmetry and the enhanced couplings of the qubit to the resonator

We consider the situation in which an external magnetic field is applied to the qubit and the magnetic flux Φ_{ext}^q is split into two parts, i.e., a perturbation part oscillating at a frequency ω_f and a fixed offset $\bar{\phi}$. Thus, the flux can be expressed as $\Phi_{\text{ext}}^q = \bar{\phi} + \phi_0 \cos \omega_f t$. If we choose $\bar{\phi} = \Phi_0/2$, the magnetic energy bias $\bar{\varepsilon}$ is just proportional to the oscillating part, resulting in the periodic breaking of the qubit inversion symmetry. In this case, the free Hamiltonian of the

qubit becomes [51]

$$H'_q = \frac{1}{2}\bar{\omega}_q\bar{\sigma}_z + \frac{1}{2}\bar{\epsilon}(\phi_0)(e^{i\omega_f t} + e^{-i\omega_f t})\bar{\sigma}_x. \quad (5)$$

In a frame rotating at half the parametric drive frequency $\omega_p/2 = \omega_f$ and neglecting the fast-oscillating terms, the Hamiltonian of the whole system takes the form

$$H = \delta_r a^\dagger a + \frac{1}{2}\delta_q\bar{\sigma}_z + \frac{1}{2}\bar{\epsilon}(\phi_0)\bar{\sigma}_x - \frac{\lambda(t)}{2}(a^{\dagger 2} + a^2) + g(a\bar{\sigma}_+ + a^\dagger\bar{\sigma}_-), \quad (6)$$

where $\delta_r = \omega_r - \omega_p/2$ and $\delta_q = \bar{\omega}_q - \omega_p/2$ are the resonator and qubit detunings, respectively.

Next, we perform a single-mode antisqueezing transformation $U(t) = e^{\frac{r(t)}{2}(a^2 - a^{\dagger 2})}$ with $\tanh 2r(t) = \lambda(t)/\delta_r$, leading to the Hamiltonian in the time-dependent squeezed frame [47,48]

$$H_s = U(t)HU^\dagger(t) - iU(t)\dot{U}^\dagger = H_f + H'_{\text{int}} + H_e, \quad (7)$$

where

$$H_f = \delta_r^s a^\dagger a + \frac{1}{2}\delta_q\bar{\sigma}_z + \frac{1}{2}\bar{\epsilon}(\phi_0)\bar{\sigma}_x, \\ H'_{\text{int}} = \bar{g}(a^\dagger + a)(\bar{\sigma}_+ + \bar{\sigma}_-) + \tilde{g}(a^\dagger - a)(\bar{\sigma}_+ - \bar{\sigma}_-), \\ H_e = i\frac{\dot{r}(t)}{2}(a^2 - a^{\dagger 2}), \quad (8)$$

where $\bar{g} = ge^{r(t)}/2$ and $\tilde{g} = ge^{-r(t)}/2$. Here the Hamiltonian H_f represents the free part with the transformed resonator detuning $\delta_r^s = \delta_r/\cosh 2r$. In the interaction Hamiltonian H'_{int} , the parameter \bar{g} in the first term denotes the effective qubit-resonator coupling strength, which is exponentially enhanced by $e^{r(t)}/2$. The second term is suppressed by $e^{-r(t)}/2$ and can be dropped in the large-amplification limit $e^{-r(t)} \rightarrow 0$. The Hamiltonian H_e provides an undesired correct term, vanishing explicitly when the drive amplitude $r(t)$ is independent of time.

By introducing the eigenstates of the qubit part, i.e., the ground state $|g\rangle = -\cos\frac{\theta}{2}|\bar{g}\rangle + \sin\frac{\theta}{2}|\bar{e}\rangle$ and the excited state $|e\rangle = \sin\frac{\theta}{2}|\bar{g}\rangle + \cos\frac{\theta}{2}|\bar{e}\rangle$, with $\theta = \arctan\frac{\bar{\epsilon}}{\delta_q}$, the Hamiltonian of the whole system becomes

$$H'_s = \delta_r^s a^\dagger a + \frac{1}{2}\omega_q\sigma_z + g_x(a + a^\dagger)\sigma_x + g_z(a + a^\dagger)\sigma_z, \quad (9)$$

where $g_x = -\bar{g}\cos\theta$, $g_z = \bar{g}\sin\theta$, $\sigma_z = |e\rangle\langle e| - |g\rangle\langle g|$, and $\sigma_x = |e\rangle\langle g| + |g\rangle\langle e|$. $\omega_q = \sqrt{\delta_q^2 + \bar{\epsilon}^2}$ is the transition frequency between the ground and excited states.

C. Creation of the superposition of long-lived single-mode squeezed coherent states

We consider the case that the qubit is driven by an external microwave field, which can be described by the Hamiltonian $H_d = \Omega(\sigma_+ e^{-i\Delta_d t} + \sigma_- e^{i\Delta_d t})$ in the frame rotating at half the parametric drive frequency $\omega_p/2 = \omega_f$. Here $\Delta_d = \omega_d - \omega_f$ denotes the detuning of the driving frequency ω_d to the oscillating frequency of the magnetic flux ω_f . Moving to an interaction picture via the unitary transformation $U = e^{-i(a^\dagger a + \sigma_z)\omega_q t/2}$, with $\omega = \omega_q/2 = \delta_r^s = (\Delta_d + \delta_d)/2$, the

Hamiltonian of the system takes the form

$$H_I = H_{I1} + H_{I2}, \quad (10)$$

where

$$H_{I1} = h e^{-i\omega t} + h^\dagger e^{i\omega t}, \\ H_{I2} = \Omega(\sigma_+ e^{i\delta_d t} + \sigma_- e^{-i\delta_d t}), \\ h = g_x a^\dagger \sigma_- + g_z a \sigma_z. \quad (11)$$

Under the condition $\omega \gg g_x, g_z, \Omega$, the Hamiltonian H_{I1} is largely detuned. According to the standard time-average method [52–54], the effective interaction can be obtained as

$$H_{I1}^{\text{eff}} = \frac{1}{\omega}[h^\dagger, h] = \frac{g_x^2}{\omega}(aa^\dagger\sigma_z + |g\rangle\langle g|) - \frac{2g_x g_z}{\omega}a^2\sigma_+ \\ - \frac{2g_x g_z}{\omega}a^{\dagger 2}\sigma_- - g_z^2 \\ = \frac{2g_x^2}{\omega}a^\dagger a |e\rangle\langle e| + \frac{g_x^2}{\omega}|e\rangle\langle e| - \frac{g_x^2}{\omega}a^\dagger a - \frac{2g_x g_z}{\omega}a^2\sigma_+ \\ - \frac{2g_x g_z}{\omega}a^{\dagger 2}\sigma_- - g_z^2, \quad (12)$$

where the condition $|e\rangle\langle e| + |g\rangle\langle g| = 1$ has been used. In combination with the driving part H_{I2} and neglecting the constant term, the effective Hamiltonian for the whole system takes the form

$$\bar{H}_{\text{eff}} = H_{I1}^{\text{eff}} + H_{I2} \\ = \frac{2g_x^2}{\omega}a^\dagger a |e\rangle\langle e| + \frac{g_x^2}{\omega}|e\rangle\langle e| - \frac{g_x^2}{\omega}a^\dagger a \\ - \frac{2g_x g_z}{\omega}(a^2\sigma_+ + a^{\dagger 2}\sigma_-) \\ + \Omega(\sigma_+ e^{i\delta_d t} + \sigma_- e^{-i\delta_d t}). \quad (13)$$

To make further progress, it is instructive to switch to a rotating frame via a unitary transformation of the form $U = e^{ig_x^2(2|e\rangle\langle e| + a^\dagger a)/\omega}$, with $\delta_d = 2g_x^2/\omega$, resulting in

$$H_{\text{eff}} = \frac{2g_x^2}{\omega}a^\dagger a |e\rangle\langle e| + \frac{3g_x^2}{\omega}|e\rangle\langle e| - \frac{2g_x g_z}{\omega}(a^2\sigma_+ + a^{\dagger 2}\sigma_-) \\ + \Omega(\sigma_+ + \sigma_-). \quad (14)$$

Note that the nonlinear coupling term in the above Hamiltonian allows the conversion of single excitations of the qubit into pairs of photons of the resonator and vice versa. Such a two-photon interaction has been widely used to explore fundamental quantum-optical phenomena, e.g., nonclassical state creation, transmission-based noise spectroscopy, and photon blockade [55–59].

In the case that the resonator exhibits a high quality factor while the qubit is largely damped via a harmonic oscillator environment in the Markovian approximation, the dynamics of the system without photon leakage of the resonator is governed by the following master equation:

$$\frac{d\rho}{dt} = -i[H_{\text{eff}}, \rho] + \frac{\gamma}{2}\mathcal{L}[\sigma_-]\rho, \quad (15)$$

where ρ denotes the system density operator, $\mathcal{L}[o]\rho = 2o\rho o^\dagger - o^\dagger o\rho - \rho o^\dagger o$ is the standard Lindblad operator for a given operator o , and γ represents the intrinsic decay rate of

the qubit. From the above equation, we can find that, on the one hand, the qubit continuously extracts photon pairs from the resonator via the two-photon exchange process and then decays to its ground state due to its energy relaxation. On the other hand, the external driving field can resonantly drive the qubit back into the excited state and then send photon pairs to the resonator. The competition of the two processes enables the system to evolve to a steady state $|\Phi_s\rangle = |\phi_s\rangle \otimes |\psi_s\rangle$, with $|\phi_s\rangle$ and $|\psi_s\rangle$ denoting the steady states of the qubit and the resonator, respectively. By setting $d\rho_s/dt = 0$, with $\rho_s = |\Phi_s\rangle\langle\Phi_s|$, we can get the equation that the steady state satisfies, i.e., $H_{\text{eff}}|\Phi_s\rangle = 0$. In the presence of large qubit dissipation, the steady state of the qubit is obviously its ground state, namely, $|\phi_s\rangle = |g\rangle$. In this case, the steady state of the resonator can be obtained by direct calculation:

$$|\psi_s\rangle = N_+|\alpha\rangle + N_-|-\alpha\rangle, \quad (16)$$

which is the superposition of the coherent states for a single mode, also called a Schrödinger cat state. Note that here $\alpha = \sqrt{\frac{\Omega\omega}{2g_x g_z}}$ is a complex amplitude, and N_+ and N_- can be arbitrary constants. Since the decay of the qubit is used as a resource for generating the target state, the state creation is robust against qubit dephasing.

Note that in the absence of resonator dissipation, the pairwise exchange of photons between the resonator and the qubit conserves the photon-number parity of the resonator mode, which is described by the so-called photon-number parity operator $P = e^{i\pi a^\dagger a}$. Such an operator plays a key role in describing the nonclassical features of electromagnetic fields, admitting the photon-number Fock states or the Schrödinger cat states as eigenstates with only two eigenvalues, $+1$ (even parity) or -1 (odd parity). Therefore, the steady state of the resonator is dependent on the photon-number parity of its initial state. For instance, the resonator will be driven into the even cat state $|\psi_s^+\rangle = (|\alpha\rangle + |-\alpha\rangle)/\sqrt{2(1 + e^{-2|\alpha|^2})}$ if the resonator is prepared in the even-parity state $|0\rangle$ at the initial time, while the initial state $|1\rangle$ with odd parity leads to the odd cat state $|\psi_s^-\rangle = (|\alpha\rangle - |-\alpha\rangle)/\sqrt{2(1 + e^{-2|\alpha|^2})}$. However, the action of the photon annihilation operator a on the system states, i.e., a photon loss, will transform an odd cat state into an even cat state and vice versa, resulting in a statistical mixture of $|\alpha\rangle$ and $|-\alpha\rangle$ and the destruction of the coherence. The high quality factor of the resonator is a necessary condition which guarantees that the photon-pair exchange rate between the resonator and the qubit can far exceed the single-photon decay, enabling the dominance of the two-photon drive and dissipation process in the system dynamic evolution and thus the maintenance of the coherence.

To verify the validity of the above discussion and study the effect of the photon leakage and the qubit dephasing, we introduce fidelity $F = \text{Tr}[\rho_{\text{tar}}\rho(t)]$ to measure the overlap between the evolved state $\rho(t)$ and the target state $\rho_{\text{tar}} = |\psi_s\rangle\langle\psi_s|$ and numerically solve the master equation (15) with two additional dissipator terms, $\frac{\kappa}{2}\mathcal{L}[a]\rho$ and $\frac{\gamma_\phi}{2}\mathcal{L}[\sigma_z]\rho$, where κ is the decay rate of the resonator and γ_ϕ is the dephasing rate of the qubit. The numerical results of fidelity F for different decay rates κ with $\gamma_\phi = 0$ are displayed in Fig. 2(a) with the system initially prepared in the ground state $|0, g\rangle$ [60]. The target state is $|\psi_s^+\rangle$, and the parameters are chosen

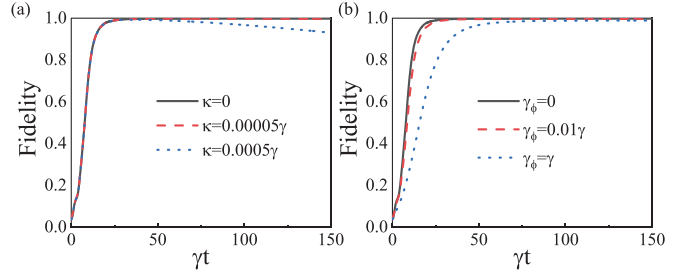


FIG. 2. Time evolution of fidelity F vs the dimensionless time γt by numerically solving the master equation (15) with two additional dissipator terms (a) for different κ with $\gamma_\phi = 0$ and (b) for different γ_ϕ with $\kappa = 0$.

as $\omega/2\pi = 2$ GHz, $\omega_q/2\pi = 4$ GHz, $\bar{g}/2\pi = 0.1$ GHz, $\theta = \pi/4$, $\Omega/2\pi = 0.02$ GHz, $\alpha = 2i$, and $\gamma/2\pi = 0.02$ GHz. It can be found that fidelity F eventually converges to $F \sim 1$ in the absence of photon leakage ($\kappa = 0$, black solid line), suggesting that the target state could be successfully created at steady state. In the case of small dissipation ($\kappa = 0.0001\gamma$, red dashed line), fidelity just slightly deviates from the ideal case, which means that the two-photon drive and dissipation process still dominates the system dynamics and thus allows for the creation of the long-lived target state. For $\kappa = 0.0005\gamma$ (blue dotted line), fidelity gradually decreases as time goes on, showing the continuous destruction of the coherence with the resonator heavily damped. In Fig. 2(b), the time evolution of the fidelity F is depicted for different dephasing rates γ_ϕ with $\kappa = 0$. It can be readily seen that F can reach a very high value close to 1 even in the large-dephasing situation ($\gamma_\phi = \gamma$, blue dotted line), showing the robustness of the scheme against qubit dephasing. Note that the nonlinear coupling strength in the simulation can be calculated as $\bar{g}^2/\omega \sim 2\pi \times 30$ MHz, which is about 2 orders of magnitude larger than that obtained from the cross-Kerr effect [9,18,61,62].

By reversing the squeezing transformation, the steady state of the resonator takes the form

$$\begin{aligned} |\psi_{\text{sc}}^\pm\rangle &= e^{\frac{r}{2}(a^{\dagger 2} - a^2)} |\psi_s^\pm\rangle \\ &= N_+ e^{\frac{r}{2}(a^{\dagger 2} - a^2)} |\alpha\rangle \pm N_- e^{\frac{r}{2}(a^{\dagger 2} - a^2)} |-\alpha\rangle, \end{aligned} \quad (17)$$

which means that for a resonator initially prepared in a state with a determined photon-number parity, the desired superposition of squeezed coherence states for a single mode, also called squeezed cat states, can be finally obtained. In comparison with a cat state, squeezing does not affect the macroscopicity of the superposition and makes the states more robust against decoherence. To characterize the nonclassical property of the created states, we introduce the Wigner function, which contains complete information about the system and can be defined as [63]

$$W(\beta) = \frac{2}{\pi} \text{Tr}[D(-\beta)\rho_a(t)D(\beta)P], \quad (18)$$

where $D[\beta] = e^{\beta a^\dagger - \beta^* a}$ is the displacement operator and $\rho_a(t)$ is the reduced density operator describing the quantized field in the resonator. The complex β plane plays the role of phase space; i.e., the real and imaginary parts of β correspond to position (x) and momentum (p) variables, respectively. It can

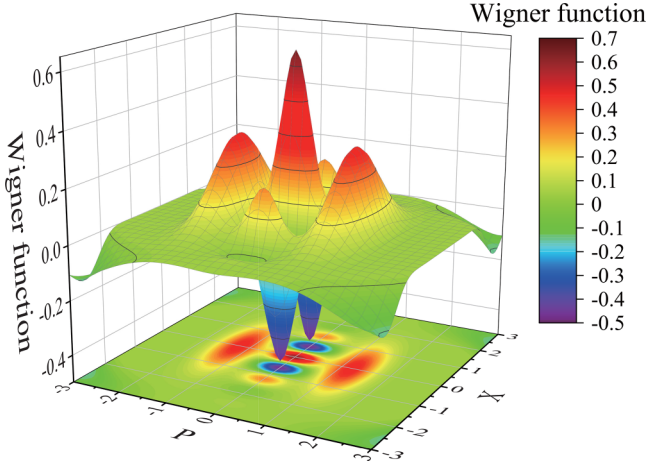


FIG. 3. Wigner function of the created steady state in the absence of resonator dissipation with $r = 0.5$.

be seen that the Wigner function at an arbitrary point β is just the expectation value of the parity operator P of the translated field of the reduced density operator $D(-\beta)\rho_a(t)D(\beta)$. The Wigner function of the created steady state is shown in Fig. 3 in the absence of cavity dissipation, where the squeezing parameter r is chosen to be a moderate value $r = 0.5$ and the initial state of the resonator and the other parameters are chosen to be the same as those in Fig. 2. We can clearly see the negative values and several quantum phase-space interference fringes between the “dead” ($|\alpha\rangle$) and “alive” ($|\alpha\rangle$) components, denoted by two red positive peaks, implying nonclassical quantum features of the created state and a real quantum superposition. In addition, we can find that the created state is squeezed along the p quadrature and stretched along the x quadrature in the presence of parametric driving.

III. CREATION OF THE SUPERPOSITION OF SQUEEZED COHERENT STATES FOR TWO MODES

In the following, we extend the above method to prepare the superposition of squeezed coherent states for microwave fields in two resonators, which can be realized in setups designed in two different ways.

A. Qubit coupled to two coupled resonators

As shown in Fig. 4, the considered setup is composed of a superconducting qubit and two TLR resonators. The two resonators interact with each other via coherent photon exchange, and one of them is coupled to the qubit. The Hamiltonian of

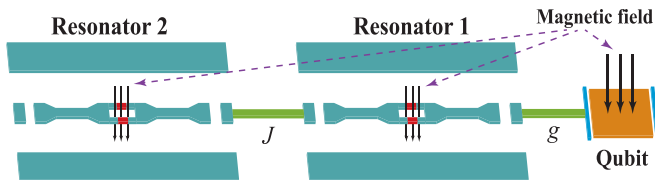


FIG. 4. Schematic diagram of a superconducting qubit coupled to two coupled TLR resonators.

the whole system can be written as

$$H = \sum_{k=1,2} (H_{rk} + H_{dk}) + H_q + H_{qr} + H_{rr}, \quad (19)$$

where $H_{rk} = \omega_{rk} a_k^\dagger a_k$ is the free Hamiltonian of the resonator k , with ω_{rk} being the resonance frequency of the resonator mode; $H_{dk} = -\lambda_k (a_k^{\dagger 2} e^{-i\omega_{pk}t} + a_k^2 e^{i\omega_{pk}t})/2$ is the corresponding parametric driving; H_q is the free Hamiltonian of the qubit given by Eq. (3); $H_{qr} = g(a_1 \bar{\sigma}_+ + a_1^\dagger \bar{\sigma}_-)$ describes the interaction between the qubit and resonator 1; and $H_{rr} = J(a_2^\dagger a_1 + a_1^\dagger a_2)$ denotes the coupling of resonator 1 to resonator 2, with J being the coupling strength. When an external magnetic field is applied to the qubit to break its inversion symmetry, the above Hamiltonian in the frame rotating at half the parametric drive frequency can be expressed as

$$\begin{aligned} H' = & \sum_{k=1,2} \delta_{rk} a_k^\dagger a_k + \frac{1}{2} \delta_q \bar{\sigma}_z + \frac{1}{2} \bar{\epsilon}(\phi_0) \bar{\sigma}_x \\ & - \frac{\lambda_1(t)}{2} (a_1^{\dagger 2} + a_1^2) - \frac{\lambda_2(t)}{2} (a_2^{\dagger 2} + a_2^2) \\ & + g(a_1 \bar{\sigma}_+ + a_1^\dagger \bar{\sigma}_-) + J(a_2^\dagger a_1 + a_1^\dagger a_2), \end{aligned} \quad (20)$$

where the condition $\omega_{p1} = \omega_{p2} = \omega_p$ has been used, resulting in the relation $\delta_{rk} = \omega_{rk} - \omega_p/2$. Under the antisqueezing transformation for each mode $U(t) = U_1(t)U_2(t)$, with $U_k(t) = e^{\frac{r_k(t)}{2}(a_k^2 - a_k^{\dagger 2})}$ and $\tan 2r_k = \lambda_k/\delta_{rk}$, the above equation becomes

$$\begin{aligned} H_s = & \sum_{k=1,2} \delta_{rk}^s a_k^\dagger a_k + \frac{1}{2} \delta_q \bar{\sigma}_z + \frac{1}{2} \bar{\epsilon}(\phi_0) \bar{\sigma}_x \\ & + \bar{g}(a^\dagger + a)(\bar{\sigma}_+ + \bar{\sigma}_-) + \bar{J}(a_2^\dagger a_1 + a_1^\dagger a_2), \end{aligned} \quad (21)$$

where $\delta_{rk}^s = \delta_{rk}/\cosh 2r_k$, $\bar{g} = g e^{r_1}/2$, and $\bar{J} = (e^{r_1+r_2} + e^{-r_1-r_2})/2$. On the basis of the qubit eigenstates $\{|g\rangle, |e\rangle\}$, the Hamiltonian can be written as

$$\begin{aligned} H_s = & \sum_{k=1,2} \delta_{rk}^s a_k^\dagger a_k + \frac{1}{2} \omega_q \sigma_z + g_x (a^\dagger + a) \sigma_x \\ & + g_z (a^\dagger + a) \sigma_z + \bar{J}(a_2^\dagger a_1 + a_1^\dagger a_2), \end{aligned} \quad (22)$$

where $g_x = -\bar{g} \cos \theta$ and $g_z = \bar{g} \sin \theta$. Here we can see that the coupling between the two resonators and that of the qubit to resonator 1 can be greatly enhanced via the parametric drivings for large r_1 and r_2 .

After introducing canonical transformations $A_1 = (a_1 + a_1^\dagger)/\sqrt{2}$ and $A_2 = (a_1 - a_2^\dagger)/\sqrt{2}$, the above Hamiltonian takes the form

$$\begin{aligned} H'_s = & (\omega + \bar{J}) A_1^\dagger A_1 + (\omega - \bar{J}) A_2^\dagger A_2 + \frac{\omega_q}{2} \sigma_z \\ & + \frac{\Delta}{2} (A_1^\dagger A_2 + A_2^\dagger A_1) + \frac{g_x}{\sqrt{2}} (A_1 + A_2 + A_1^\dagger + A_2^\dagger) \sigma_x \\ & + \frac{g_z}{\sqrt{2}} (A_1 + A_2 + A_1^\dagger + A_2^\dagger) \sigma_z, \end{aligned} \quad (23)$$

where $\omega = (\delta_{r1}^s + \delta_{r2}^s)/2$ and $\Delta = \delta_{r1}^s - \delta_{r2}^s$. In the presence of a driving field applied to the qubit (Hamiltonian H_d) and by switching to the interaction picture via the unitary transformation $U = e^{-i[(\omega + \bar{J})A_1^\dagger A_1 + (\omega - \bar{J})A_2^\dagger A_2 + \omega_q \sigma_z/2]t}$, with $\omega_q = 2(\omega + \bar{J})$

and $\Delta' = \Delta_d - \omega_q$, we have

$$\begin{aligned}
 H_I = & \frac{g_x}{\sqrt{2}}(A_1\sigma_+e^{i(\omega+\bar{J})t} + A_2\sigma_+e^{i(\omega+2\bar{J})t}) \\
 & + \frac{g_z}{\sqrt{2}}(A_1\sigma_z e^{-i(\omega+\bar{J})t} + A_2\sigma_z e^{i(\omega-\bar{J})t}) + \text{H.c.} \\
 & + \frac{\Delta}{2}(A_1^\dagger A_2 e^{2i\bar{J}t} + A_2^\dagger A_1 e^{-2i\bar{J}t}) + \Omega(\sigma_+ e^{-i\Delta't} + \sigma_- e^{i\Delta't}).
 \end{aligned} \quad (24)$$

In the case that $\omega \pm \bar{J} \gg g_x/\sqrt{2}, g_z/\sqrt{2}$, the following effective Hamiltonian can be obtained by using the standard time-average method:

$$\begin{aligned}
 H_{\text{eff}} = & \frac{g_x^2}{2(\omega + \bar{J})} A_1^\dagger A_1 \sigma_z + \frac{g_x^2}{2(\omega + 2\bar{J})} A_2^\dagger A_2 \sigma_z \\
 & + \left(\frac{g_x^2}{2(\omega + \bar{J})} + \frac{g_x^2}{2(\omega + 2\bar{J})} \right) |e\rangle\langle e| \\
 & + \frac{\Delta}{2} (A_1^\dagger A_2 e^{2i\bar{J}t} + A_2^\dagger A_1 e^{-2i\bar{J}t}) \\
 & - \frac{g_x g_z}{\omega + \bar{J}} A_1^2 \sigma_+ - \frac{g_x g_z}{\omega + \bar{J}} A_1^{\dagger 2} \sigma_- \\
 & + \Omega(\sigma_+ e^{-i\Delta't} + \sigma_- e^{i\Delta't}).
 \end{aligned} \quad (25)$$

Performing a new unitary transformation $U = e^{-iH_0 t}$, with $H_0 = -g_x^2(A_1^\dagger A_1 + 2|e\rangle\langle e|)/2(\omega + \bar{J})$ and $\Delta' = -g_x^2/(\omega + \bar{J})$, the above Hamiltonian becomes

$$\begin{aligned}
 H'_{\text{eff}} = & \frac{g_x^2}{\omega + \bar{J}} A_1^\dagger A_1 |e\rangle\langle e| + \frac{g_x^2}{2(\omega + 2\bar{J})} A_2^\dagger A_2 \sigma_z \\
 & + \left(\frac{3g_x^2}{2(\omega + \bar{J})} + \frac{g_x^2}{2(\omega + 2\bar{J})} \right) |e\rangle\langle e| \\
 & - \frac{g_x g_z}{\omega + \bar{J}} A_1^2 \sigma_+ - \frac{g_x g_z}{\omega + \bar{J}} A_1^{\dagger 2} \sigma_- + \Omega(\sigma_+ + \sigma_-) \\
 & + \frac{\Delta}{2} (A_1^\dagger A_2 e^{i(2\bar{J} - \frac{g_x^2}{2(\omega+\bar{J})})t} + A_2^\dagger A_1 e^{i(2\bar{J} - \frac{g_x^2}{2(\omega+\bar{J})})t}).
 \end{aligned} \quad (26)$$

Under the condition $2\bar{J} - \frac{g_x^2}{2(\omega+\bar{J})} \gg \Delta$, the single-photon exchange between modes A_1 and A_2 can be neglected, and the above Hamiltonian finally reduces to

$$\begin{aligned}
 H_{\text{eff}} = & \frac{g_x^2}{\omega + \bar{J}} A_1^\dagger A_1 |e\rangle\langle e| + \left(\frac{3g_x^2}{2(\omega + \bar{J})} + \frac{g_x^2}{2(\omega + 2\bar{J})} \right) |e\rangle\langle e| \\
 & - \frac{g_x g_z}{\omega + \bar{J}} (A_1^2 \sigma_+ + A_1^{\dagger 2} \sigma_-) + \Omega(\sigma_+ + \sigma_-).
 \end{aligned} \quad (27)$$

Similar to Eq. (14), the above Hamiltonian enables pairwise exchange of photons between the qubit and mode A_1 , which is crucial for state preparation.

In the absence of resonator dissipation, the time evolution of the density operator for the system can be described by the following master equation:

$$\frac{d\rho}{dt} = -i[H_{\text{eff}}, \rho] + \frac{\gamma}{2} \mathcal{L}[\sigma_-]\rho. \quad (28)$$

Similarly, the dissipation-repumping process can drive the system into a steady state $|\Phi_s\rangle = |g\rangle \otimes |\psi_s\rangle$ for large qubit dissipation. Direct calculations show that the steady state of the resonators $|\psi_s\rangle$ is a two-mode Schrödinger cat state, which

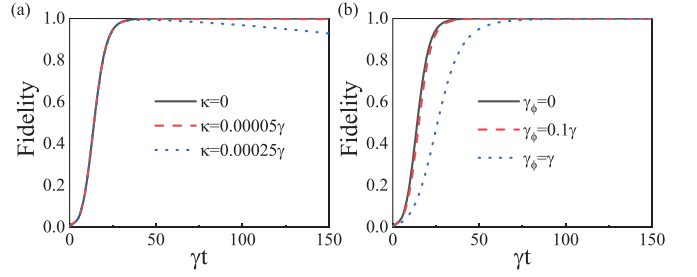


FIG. 5. Time evolution of fidelity F vs the dimensionless time γt simulated using the Hamiltonian in Eq. (27) (a) for different κ with $\gamma_{\phi=0}$ and (b) for different γ_{ϕ} with $\kappa = 0$.

should be one of the eigenstates of the operator $e^{i\pi A_1^\dagger A_1}$ with eigenvalues $+1$ and -1 , depending on the parity of the initial state. For example, when the system is initially prepared in an even-parity state $|0, 0\rangle$, i.e., both of the resonators are in the vacuum states, the steady state of the resonators can be described by

$$|\psi_s^+\rangle = (|\alpha, \alpha\rangle + |-\alpha, -\alpha\rangle) / \sqrt{2(1 + e^{-4|\alpha|^2})}, \quad (29)$$

which is the superposition of coherent states for two resonator modes with $\alpha = \sqrt{\frac{\Omega(\omega+\bar{J})}{2g_x g_z}}$, i.e., a two-mode cat state with even parity. For the system prepared in an odd-parity state $(|0, 1\rangle + |1, 0\rangle)/\sqrt{2}$ at the initial time, the steady state of the two resonators takes the form

$$|\psi_s^-\rangle = (|\alpha, \alpha\rangle - |-\alpha, -\alpha\rangle) / \sqrt{2(1 + e^{-4|\alpha|^2})}, \quad (30)$$

which is just a two-mode cat state with odd parity. In comparison with single-mode cat states, two-mode cat states can significantly increase the quantum information capacity and have been widely used as an import resource in diverse areas ranging from quantum metrology [64] to quantum teleportation [65].

As shown in Fig. 5, fidelity F is calculated by numerically solving the master equation (28) with three additional dissipator terms: $\frac{\kappa_1}{2} \mathcal{L}[a_1]\rho$, $\frac{\kappa_2}{2} \mathcal{L}[a_2]\rho$, and $\frac{\gamma_{\phi}}{2} \mathcal{L}[\sigma_z]\rho$, where κ_1 and κ_2 denote the decay rates of the two resonators. The system is initially prepared in the odd-parity state $(|0, 1\rangle + |1, 0\rangle)/\sqrt{2}$; thus, the target state is the two-mode cat state $|\psi_s^-\rangle$ expressed by Eq. (30). The parameters are set as $\omega/2\pi = 1.8$ GHz, $\bar{J} = 0.2$ GHz, and $\kappa = \kappa_1 = \kappa_2$; other parameters are the same as in Fig. 2. It can be clearly seen from Fig. 5(a) that the target state can be successfully created for zero ($\kappa = 0$, black solid line) and a small ($\kappa = 0.00005\gamma$, red dashed line) resonator decay rate. However, the coherence of the created state will be greatly damaged as time gets long due to the photon loss for a large decay rate ($\kappa = 0.0025\gamma$, blue dotted line). The results of fidelity F for different qubit dephasings illustrated in Fig. 5(b) also indicate that the state creation is robust against qubit dephasing.

By reversing the squeezing transformation, we can find that the steady states $|\psi_{sc}\rangle$ of the two resonators are the superposition of squeezed coherent states for two modes. For instance, if the two resonators are initially prepared in the even-parity state $|0, 0\rangle$ or the odd-parity state $(|0, 1\rangle + |1, 0\rangle)/\sqrt{2}$, the

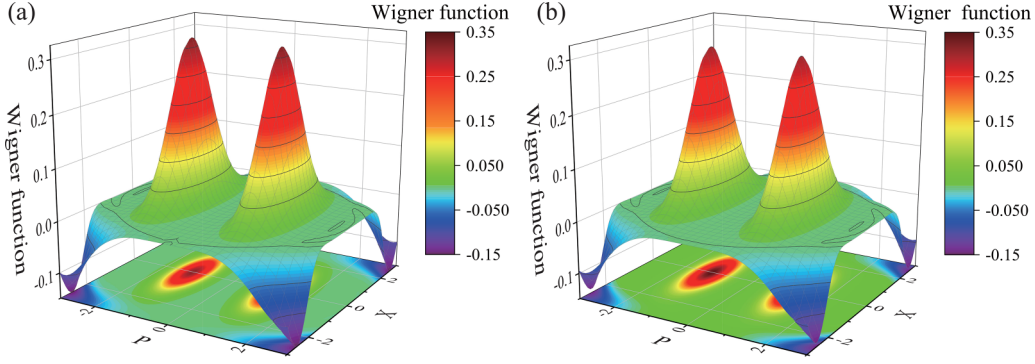


FIG. 6. Wigner function of individual resonators in the absence of resonator dissipation of (a) resonator 1 and (b) resonator 2.

corresponding steady states take the form

$$|\psi_{\text{sc}}^{\pm}\rangle = [U_2^{\dagger}(t)U_1^{\dagger}(t)|\alpha, \alpha\rangle \pm U_2^{\dagger}(t)U_1^{\dagger}(t)|-\alpha, -\alpha\rangle] / \sqrt{2(1 + e^{-4|\alpha|^2})}. \quad (31)$$

Different from the superposition of squeezed coherent states for a single mode, the nonclassical property of the superposition of squeezed coherent states for two modes cannot be fully shown by the Wigner function of individual resonator modes. In Figs. 6(a) and 6(b), we depict the Wigner functions of resonator 1 and resonator 2, respectively, for the created state in the absence of resonator dissipation with $r = 0.5$. Compared with the superposition of squeezed coherent states for a single mode shown in Fig. 3, the two components and the squeezing along the p quadrature and the stretching along the x quadrature of the generated state in both plots can still clearly be seen; however, the quantum phase-space interference fringes vanish, exhibiting the statistical mixture of two coherent states and the lack of full quantum information on the global quantum state. To address this issue, we introduce the joint Wigner function, defined by [66]

$$W_J = \frac{4}{\pi^2} \text{Tr}[\rho_{a_1 a_2} D_1(\beta_1) D_2(\beta_2) P_J D_1(-\beta_1) D_2(-\beta_2)], \quad (32)$$

where $\rho_{a_1 a_2}$ denotes the reduced operator of the resonator modes, $D_k(\beta_k) = e^{\beta_k a_k^{\dagger} - \beta_k^* a_k}$ represents the displacement operator for the a_k mode with complex parameter β_k , and $P_J = P_1 P_2 = e^{i\pi a_1^{\dagger} a_1} e^{i\pi a_2^{\dagger} a_2}$ is the joint photon-number parity operator. It can readily be seen that the joint Wigner function is a function in the four-dimensional phase space $\{\text{Re}(\beta_1), \text{Im}(\beta_1), \text{Re}(\beta_2), \text{Im}(\beta_2)\}$. To globally display the core features of the created state, the joint Wigner function is calculated numerically, and its two-dimensional cuts along the $\text{Im}(\beta_1) - \text{Im}(\beta_2)$ plane and the $\text{Re}(\beta_1) - \text{Re}(\beta_2)$ plane are illustrated in Figs. 7(a) and 7(b), respectively. The two red peaks in Fig. 7(a) denote the probability distribution of the two coherent-state components, while the central blue peak and the fringes with strong negativity in Fig. 7(b) demonstrate the quantum interference between the two components and the nonclassical property of the global quantum state. Compared with the two-mode cat states without squeezing, the created state is squeezed along the $\text{Im}(\beta_1) - \text{Im}(\beta_2)$ plane and stretched along the $\text{Re}(\beta_1) - \text{Re}(\beta_2)$ plane.

B. Qubit coupled to two separated resonators

As illustrated in Fig. 8, the setup under consideration consists of a superconducting qubit coupled to two separated TLR resonators, with g_k being the coupling strength to the resonator k . The total Hamiltonian in the frame rotating at half the parametric drive frequency can be written as

$$H = \sum_{k=1,2} \delta_{rk} a_k^{\dagger} a_k + \frac{1}{2} \delta_q \bar{\sigma}_z + \frac{1}{2} \bar{\epsilon}(\phi_0) \bar{\sigma}_x - \frac{\lambda_1(t)}{2} (a_1^{\dagger 2} + a_1^2) - \frac{\lambda_2(t)}{2} (a_2^{\dagger 2} + a_2^2) + g_1 (a_1 \bar{\sigma}_+ + a_1^{\dagger} \bar{\sigma}_-) + g_2 (a_2 \bar{\sigma}_+ + a_2^{\dagger} \bar{\sigma}_-). \quad (33)$$

Under the antisqueezing transformation for each mode $U(t) = U_1(t)U_2(t)$, with $U_k(t) = e^{\frac{r_k(t)}{2}(a_k^{\dagger 2} - a_k^2)}$ and $\tan 2r_k = \lambda_k / \delta_{rk}$, the above equation can be described by

$$H = \sum_{k=1,2} \delta_{rk}^s a_k^{\dagger} a_k + \frac{1}{2} \delta_q \bar{\sigma}_z + \frac{1}{2} \bar{\epsilon}(\phi_0) \bar{\sigma}_x + \sum_{k=1,2} \bar{g}_k (a_k + a_k)(\bar{\sigma}_+ + \bar{\sigma}_-), \quad (34)$$

with $\bar{g}_k = g_k e^{r_k} / 2$. On the basis of the qubit eigenstates, the above Hamiltonian takes the form

$$H = \sum_{k=1,2} \delta_{rk}^s a_k^{\dagger} a_k + \frac{1}{2} \omega_q \sigma_z + \sum_{k=1,2} (a_k + a_k)(g_{kx} \sigma_x + g_{kz} \sigma_z), \quad (35)$$

where $g_{kx} = -\bar{g}_k \cos \theta$ and $g_{kz} = \bar{g}_k \sin \theta$. Introducing the canonical transformations $A_1 = (a_1 + a_1^{\dagger}) / \sqrt{2}$ and $A_2 = (a_1 - a_2^{\dagger}) / \sqrt{2}$ in the presence of the driving field H_d applied to the qubit, the above Hamiltonian becomes

$$H' = \omega (A_1^{\dagger} A_1 + A_2^{\dagger} A_2) + \frac{\Delta}{2} (A_1^{\dagger} A_2 + A_2^{\dagger} A_1) + \frac{1}{2} \omega_q \sigma_z + \sqrt{2} g_x (A_1 + A_1^{\dagger}) \sigma_x + \sqrt{2} g_z (A_1 + A_1^{\dagger}) \sigma_z + \Omega (\sigma_+ e^{-i\Delta t} + \sigma_- e^{i\Delta t}), \quad (36)$$

where $g_x = g_{1x} = g_{2x}$, $g_z = g_{1z} = g_{2z}$, $\omega = (\delta_{r_1}^s + \delta_{r_1}^s) / 2$, and $\Delta = (\delta_{r_1}^s - \delta_{r_1}^s) / 2$. In the case that $\Delta = 0$, the dynamics of the system is independent of the mode A_2 ; thus, the above Hamiltonian is similar to Eq. (9) with the driving term H_d ,

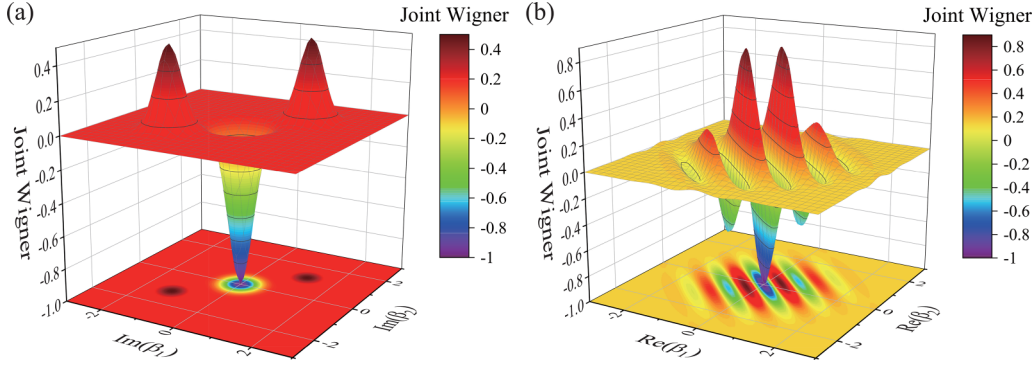


FIG. 7. Two-dimensional cuts of the joint Wigner function of the generated state along (a) the $\text{Im}(\beta_1) - \text{Im}(\beta_2)$ plane and (b) the $\text{Re}(\beta_1) - \text{Re}(\beta_2)$ plane in the absence of resonator dissipation.

leading to the following effective Hamiltonian:

$$H_{\text{eff}} = \frac{4g_x^2}{\omega} A_1^\dagger A_1 |e\rangle\langle e| + \frac{2g_x^2}{\omega} |e\rangle\langle e| - \frac{4g_x g_z}{\omega} A_1^2 \sigma_+ - \frac{4g_x g_z}{\omega} A_1^{\dagger 2} \sigma_- + \Omega(\sigma_+ + \sigma_-). \quad (37)$$

When the qubit is heavily damped, the steady state of the system can also be described by $|\Phi_s\rangle = |g\rangle \otimes |\psi_s\rangle$, with $|\psi_s\rangle$ being a two-mode Schrödinger cat state depending on the parity of its initial state. For the two resonators initially prepared in an even-parity state $|0, 0\rangle$ and an odd-parity state $(|0, 1\rangle + |1, 0\rangle)/\sqrt{2}$, the steady state $|\psi_s\rangle$ can be expressed by $|\psi_s^\pm\rangle$ given by Eqs. (29) and (30) with $\alpha = \frac{1}{2}\sqrt{\frac{\Omega\omega}{2g_x g_z}}$, respectively.

Fidelity F is calculated by numerically solving the master equation (28) with three additional dissipator terms ($\frac{\kappa_1}{2}\mathcal{L}[a_1]\rho$, $\frac{\kappa_2}{2}\mathcal{L}[a_2]\rho$, and $\frac{\gamma_\phi}{2}\mathcal{L}[\sigma_z]\rho$) and H_{eff} given by Eq. (37) instead of Eq. (27). The parameters are chosen to be $\omega = 2$ GHz, $\Omega = 0.045$ GHz, and $\alpha = 1.5i$; other parameters and the initial state of the system are same as in Fig. 5. The results depicted in Fig. 9(a) illustrate that the target state can also be successfully generated for zero ($\kappa = 0$, black solid line) and a small ($\kappa = 0.00005\gamma$, red dashed line) resonator decay rate, while the coherence of the created state is continuously damaged for a large resonator decay rate ($\kappa = 0.0005\gamma$, blue dotted line). The results illustrated in Fig. 9(b) show that the state creation is robust to qubit dephasing.

By reversing the squeezing transformation, we can finally obtain the desired superposition of squeezed coherent states for two modes. As illustrated in Figs. 10(a) and 10(b), the joint Wigner function of the steady state is simulated using the Hamiltonian in Eq. (37) in the absence of resonator

dissipation. Like in Figs. 7(a) and 7(b), we can readily see the squeezed central blue feature in Fig. 10(a) and the stretched quantum interference with strong negativity in Fig. 10(b), showing highly nonclassical properties of the created state.

IV. EXPERIMENTAL FEASIBILITY

Finally, we discuss the experimental feasibility of the proposed method. In experiments, microwave resonators usually work in the 2–15-GHz microwave regime [29], while the typical transition frequencies of superconducting qubits range from hundreds of megahertz to larger than 10 GHz [38,49,51,67–69]. In our scheme, both the qubit and the resonator detunings can be further tuned via the parametric driving frequency. To obtain the target states with high fidelity, the largest value of the required quality factor of the TLRs in the simulations is about 10^7 . This condition can be readily satisfied since a TLR with a quality factor $Q > 10^7$ was fabricated [70] and a quality factor beyond 10^8 was reported in three-dimensional microwave resonators [71,72]. Experimentally, both the coupling strength of the qubit to the resonators and that between the two resonators can reach hundreds of megahertz and can be dynamically tuned [73–75]. Furthermore, we note that a squeezing parameter r larger than 1 can be achieved in superconducting quantum circuits [76,77]. Therefore, the present scheme can be implemented with currently available parameters.

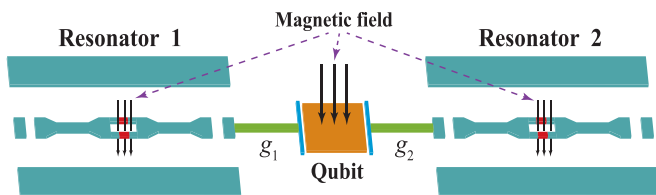


FIG. 8. Schematic diagram of a superconducting qubit simultaneously coupled to two separated TLR resonators.

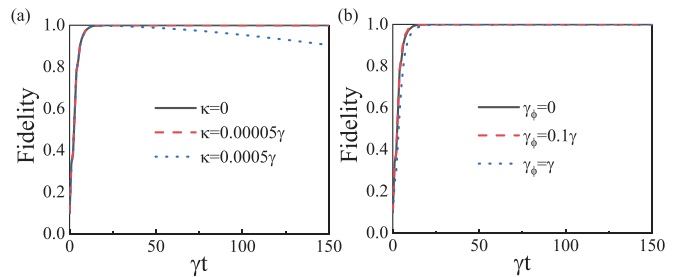


FIG. 9. Time evolution of fidelity F vs dimensionless time γt simulated using the Hamiltonian in Eq. (37) (a) for different κ with $\gamma_\phi = 0$ and (b) for different γ_ϕ with $\kappa = 0$.

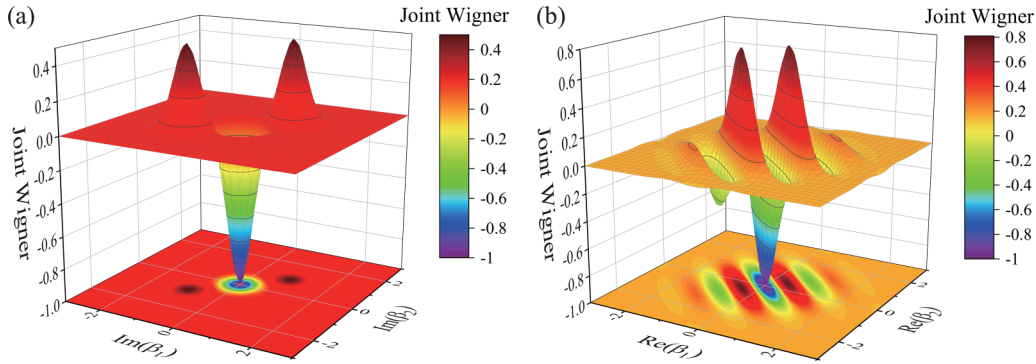


FIG. 10. Two-dimensional cuts of the joint Wigner function of the generated state along (a) the $\text{Im}(\beta_1) - \text{Im}(\beta_2)$ plane and (b) the $\text{Re}(\beta_1) - \text{Re}(\beta_2)$ plane in the absence of resonator dissipation, which is simulated using the Hamiltonian in Eq. (37).

V. CONCLUSION

In conclusion, we presented an efficient protocol for the dissipative generation of a long-lived superposition of squeezed coherent states for a single and two resonator modes. The considered setup is composed of a superconducting qubit with periodically broken inversion symmetry coupled to a single or two parametrically driven TLRs with different circuit structures. The resulting parametric-driving-enhanced transverse and longitudinal couplings of the qubit to the resonators can induce strong nonlinear two-photon interactions between the qubit and the resonators. In combination with an additional microwave drive applied on the qubit, the superposition of squeezed coherent states in the resonators can be engineered at steady state in a dissipative process. Numerical simulations showed that a target state with high fidelity and highly non-classical properties can be successfully created. In addition, our proposal can be implemented in other quantum systems

such as hybrid quantum systems combining a superconducting qubit and magnons or phonons [78–83].

ACKNOWLEDGMENTS

This work was supported by the National Natural Science Foundation of China (Grant No. 12174300), the Natural Science Foundation of Hubei Province of China (Grant No. 2020CFB748), the Natural Science Foundation of Shandong Province of China (Grants No. ZR2021MA042 and No. ZR2021MA078), the Program for Science and Technology Innovation Team in Colleges of Hubei Province of China (Grant No. T2021012), and the Doctoral Scientific Research Foundation of Hubei University of Automotive Technology (Grants No. BK202113, No. BK201906, and No. BK202008).

-
- [1] W. H. Zurek, *Nature (London)* **412**, 712 (2001).
 [2] C. Song, K. Xu, H. Li, Y.-R. Zhang, X. Zhang, W. Liu, Q. Guo, Z. Wang, W. Ren, J. Hao, H. Feng, H. Fan, D. Zheng, D.-W. Wang, H. Wang, and S.-Y. Zhu, *Science* **365**, 574 (2019).
 [3] E. Schrödinger, *Naturwissenschaften* **23**, 807 (1935).
 [4] H. Jeong, W. Son, M. S. Kim, D. Ahn, and Č. Brukner, *Phys. Rev. A* **67**, 012106 (2003).
 [5] M. Stobińska, H. Jeong, and T. C. Ralph, *Phys. Rev. A* **75**, 052105 (2007).
 [6] W. H. Zurek, *Rev. Mod. Phys.* **75**, 715 (2003).
 [7] W. J. Munro, K. Nemoto, G. J. Milburn, and S. L. Braunstein, *Phys. Rev. A* **66**, 023819 (2002).
 [8] B. Vlastakis, G. Kirchmair, Z. Leghtas, S. E. Nigg, L. Frunzio, S. M. Girvin, M. Mirrahimi, M. H. Devoret, and R. J. Schoelkopf, *Science* **342**, 607 (2013).
 [9] M. Mirrahimi, Z. Leghtas, V. V. Albert, S. Touzard, R. J. Schoelkopf, L. Jiang, and M. H. Devoret, *New J. Phys.* **16**, 045014 (2014).
 [10] S. Puri, A. Grimm, P. Campagne-Ibarcq, A. Eickbusch, K. Noh, G. Roberts, L. Jiang, M. Mirrahimi, M. H. Devoret, and S. M. Girvin, *Phys. Rev. X* **9**, 041009 (2019).
 [11] R. Lescanne, M. Villiers, T. Peronnin, A. Sarlette, M. Delbecq, B. Huard, T. Kontos, M. Mirrahimi, and Z. Leghtas, *Nat. Phys.* **16**, 509 (2020).
 [12] A. Grimm, N. E. Frattini, S. Puri, S. O. Mundhada, S. Touzard, M. Mirrahimi, S. M. Girvin, S. Shankar, and M. H. Devoret, *Nature (London)* **584**, 205 (2020).
 [13] A. Ourjoumtsev, H. Jeong, R. Tualle-Brouri, and P. Grangier, *Nature (London)* **448**, 784 (2007).
 [14] P. A. Knott, T. J. Proctor, A. J. Hayes, J. P. Cooling, and J. A. Dunningham, *Phys. Rev. A* **93**, 033859 (2016).
 [15] D. S. Schlegel, F. Minganti, and V. Savona, *Phys. Rev. A* **106**, 022431 (2022).
 [16] J. Etesse, M. Bouillard, B. Kanseri, and R. Tualle-Brouri, *Phys. Rev. Lett.* **114**, 193602 (2015).
 [17] K. Huang, H. Le Jeannic, J. Ruaudel, V. B. Verma, M. D. Shaw, F. Marsili, S. W. Nam, E. Wu, H. Zeng, Y.-C. Jeong, R. Filip, O. Morin, and J. Laurat, *Phys. Rev. Lett.* **115**, 023602 (2015).
 [18] Z. Leghtas, S. Touzard, I. M. Pop, A. Kou, B. Vlastakis, A. Petrenko, K. M. Sliwa, A. Narla, S. Shankar, M. J. Hatridge, M. Reagor, L. Frunzio, R. J. Schoelkopf, M. Mirrahimi, and M. H. Devoret, *Science* **347**, 853 (2015).
 [19] R. Gautier, A. Sarlette, and M. Mirrahimi, *PRX Quantum* **3**, 020339 (2022).
 [20] X.-Y. Lü, G.-L. Zhu, L.-L. Zheng, and Y. Wu, *Phys. Rev. A* **97**, 033807 (2018).
 [21] Z. Zhang, L. Shao, W. Lu, and X. Wang, *Phys. Rev. A* **106**, 043721 (2022).

- [22] Y.-x. Liu, J. Q. You, L. F. Wei, C. P. Sun, and F. Nori, *Phys. Rev. Lett.* **95**, 087001 (2005).
- [23] Q. Bin, Y. Wu, and X.-Y. Lü, *Phys. Rev. Lett.* **127**, 073602 (2021).
- [24] Y.-J. Zhao, Y.-L. Liu, Y.-x. Liu, and F. Nori, *Phys. Rev. A* **91**, 053820 (2015).
- [25] J.-H. Park, A. Ndao, W. Cai, L. Hsu, A. Kodigala, T. Lepetit, Y.-H. Lo, and B. Kanté, *Nat. Phys.* **16**, 462 (2020).
- [26] I. Piskog, D. Fregenal, O. Frette, M. Førre, E. Horsdal, and A. Waheed, *Phys. Rev. A* **83**, 043405 (2011).
- [27] F. Martín, J. Fernández, T. Havermeier, L. Foucar, T. Weber, K. Kreidi, M. Schöffler, L. Schmidt, T. Jahnke, O. Jagutzki, A. Czasch, E. P. Benis, T. Osipov, A. L. Landers, A. Belkacem, M. H. Prior, H. Schmidt-Böcking, C. L. Cocke, and R. Dörner, *Science* **315**, 629 (2007).
- [28] O. V. Kibis, G. Y. Slepyan, S. A. Maksimenko, and A. Hoffmann, *Phys. Rev. Lett.* **102**, 023601 (2009).
- [29] X. Gu, A. F. Kockum, A. Miranowicz, Y. Liu, and F. Nori, *Phys. Rep.* **718–719**, 1 (2017).
- [30] J. Clarke and F. K. Wilhelm, *Nature (London)* **453**, 1031 (2008).
- [31] A. Blais, A. L. Grimsmo, S. M. Girvin, and A. Wallraff, *Rev. Mod. Phys.* **93**, 025005 (2021).
- [32] M. Koppenhöfer and M. Marthaler, *Phys. Rev. A* **93**, 023831 (2016).
- [33] P.-M. Billangeon, J. S. Tsai, and Y. Nakamura, *Phys. Rev. B* **92**, 020509(R) (2015).
- [34] H. Toida, T. Ohrai, Y. Matsuzaki, K. Kakuyanagi, and S. Saito, *Phys. Rev. B* **102**, 094502 (2020).
- [35] S. Richer and D. DiVincenzo, *Phys. Rev. B* **93**, 134501 (2016).
- [36] X. Wang, A. Miranowicz, H.-R. Li, and F. Nori, *Phys. Rev. B* **95**, 205415 (2017).
- [37] V. E. Manucharyan, J. Koch, L. I. Glazman, and M. H. Devoret, *Science* **326**, 113 (2009).
- [38] F. Bao, H. Deng, D. Ding, R. Gao, X. Gao, C. Huang, X. Jiang, H.-S. Ku, Z. Li, X. Ma, X. Ni, J. Qin, Z. Song, H. Sun, C. Tang, T. Wang, F. Wu, T. Xia, W. Yu, F. Zhang *et al.*, *Phys. Rev. Lett.* **129**, 010502 (2022).
- [39] Q. Ficheux, L. B. Nguyen, A. Somoroff, H. Xiong, K. N. Nesterov, M. G. Vavilov, and V. E. Manucharyan, *Phys. Rev. X* **11**, 021026 (2021).
- [40] H. Zhang, S. Chakram, T. Roy, N. Earnest, Y. Lu, Z. Huang, D. K. Weiss, J. Koch, and D. I. Schuster, *Phys. Rev. X* **11**, 011010 (2021).
- [41] A. Blais, R.-S. Huang, A. Wallraff, S. M. Girvin, and R. J. Schoelkopf, *Phys. Rev. A* **69**, 062320 (2004).
- [42] J. Q. You and F. Nori, *Phys. Today* **58**(11), 42 (2005).
- [43] T. Yamamoto, K. Inomata, M. Watanabe, K. Matsuba, T. Miyazaki, W. D. Oliver, Y. Nakamura, and J. S. Tsai, *Appl. Phys. Lett.* **93**, 042510 (2008).
- [44] C. Macklin, K. O'Brien, D. Hover, M. E. Schwartz, V. Bolkhovskiy, X. Zhang, W. D. Oliver, and I. Siddiqi, *Science* **350**, 307 (2015).
- [45] C. K. Andersen and K. Mølmer, *Phys. Rev. A* **91**, 023828 (2015).
- [46] J.-K. Xie, S.-L. Ma, Y.-L. Ren, X.-K. Li, and F.-L. Li, *Phys. Rev. A* **101**, 012348 (2020).
- [47] C. Leroux, L. C. G. Govia, and A. A. Clerk, *Phys. Rev. Lett.* **120**, 093602 (2018).
- [48] X.-Y. Lü, Y. Wu, J. R. Johansson, H. Jing, J. Zhang, and F. Nori, *Phys. Rev. Lett.* **114**, 093602 (2015).
- [49] L. B. Nguyen, Y.-H. Lin, A. Somoroff, R. Mencia, N. Grabon, and V. E. Manucharyan, *Phys. Rev. X* **9**, 041041 (2019).
- [50] P. Krantz, M. Kjaergaard, F. Yan, T. P. Orlando, S. Gustavsson, and W. D. Oliver, *Appl. Phys. Rev.* **6**, 021318 (2019).
- [51] D. K. Weiss, H. Zhang, C. Ding, Y. Ma, D. I. Schuster, and J. Koch, *PRX Quantum* **3**, 040336 (2022).
- [52] D. F. James and J. Jerke, *Can. J. Phys.* **85**, 625 (2007).
- [53] P. Li, *Phys. Rev. A* **77**, 015809 (2008).
- [54] Y.-C. Zhang, X.-F. Zhou, X. Zhou, G.-C. Guo, and Z.-W. Zhou, *Phys. Rev. Lett.* **118**, 083604 (2017).
- [55] S. Felicetti, D. Z. Rossatto, E. Rico, E. Solano, and P. Forn-Díaz, *Phys. Rev. A* **97**, 013851 (2018).
- [56] A. Kowalewska-Kudłaszuk, S. I. Abo, G. Chimeczak, J. Peřina, F. Nori, and A. Miranowicz, *Phys. Rev. A* **100**, 053857 (2019).
- [57] S. Felicetti, M.-J. Hwang, and A. Le Boité, *Phys. Rev. A* **98**, 053859 (2018).
- [58] F. Zou, X.-Y. Zhang, X.-W. Xu, J.-F. Huang, and J.-Q. Liao, *Phys. Rev. A* **102**, 053710 (2020).
- [59] P. M. Mutter and G. Burkard, *Phys. Rev. A* **107**, 052603 (2023).
- [60] J. R. Johansson, P. D. Nation, and F. Nori, *Comput. Phys. Commun.* **183**, 1760 (2012).
- [61] A. Roy, Z. Leghtas, A. D. Stone, M. Devoret, and M. Mirrahimi, *Phys. Rev. A* **91**, 013810 (2015).
- [62] S. Touzard, A. Grimm, Z. Leghtas, S. O. Mundhada, P. Reinhold, C. Axline, M. Reagor, K. Chou, J. Blumoff, K. M. Sliwa, S. Shankar, L. Frunzio, R. J. Schoelkopf, M. Mirrahimi, and M. H. Devoret, *Phys. Rev. X* **8**, 021005 (2018).
- [63] K. E. Cahill and R. J. Glauber, *Phys. Rev.* **177**, 1857 (1969).
- [64] J. Joo, W. J. Munro, and T. P. Spiller, *Phys. Rev. Lett.* **107**, 083601 (2011).
- [65] S. J. van Enk and O. Hirota, *Phys. Rev. A* **64**, 022313 (2001).
- [66] C. Wang, Y. Y. Gao, P. Reinhold, R. W. Heeres, N. Ofek, K. Chou, C. Axline, M. Reagor, J. Blumoff, K. M. Sliwa, L. Frunzio, S. M. Girvin, L. Jiang, M. Mirrahimi, M. H. Devoret, and R. J. Schoelkopf, *Science* **352**, 1087 (2016).
- [67] F. G. Paauw, A. Fedorov, C. J. P. M. Harmans, and J. E. Mooij, *Phys. Rev. Lett.* **102**, 090501 (2009).
- [68] M. J. Schwarz, J. Goetz, Z. Jiang, T. Niemczyk, F. Deppe, A. Marx, and R. Gross, *New J. Phys.* **15**, 045001 (2013).
- [69] P. M. Leung and B. C. Sanders, *Phys. Rev. Lett.* **109**, 253603 (2012).
- [70] A. Megrant, C. Neill, R. Barends, B. Chiaro, Y. Chen, L. Feigl, J. Kelly, E. Lucero, M. Mariantoni, P. J. J. O'Malley, D. Sank, A. Vainsencher, J. Wenner, T. C. White, Y. Yin, J. Zhao, C. J. Palmström, J. M. Martinis, and A. N. Cleland, *Appl. Phys. Lett.* **100**, 113510 (2012).
- [71] M. Reagor, W. Pfaff, C. Axline, R. W. Heeres, N. Ofek, K. Sliwa, E. Holland, C. Wang, J. Blumoff, K. Chou, M. J. Hatridge, L. Frunzio, M. H. Devoret, L. Jiang, and R. J. Schoelkopf, *Phys. Rev. B* **94**, 014506 (2016).
- [72] A. Romanenko, R. Pilipenko, S. Zorzetti, D. Frolov, M. Awida, S. Belomestnykh, S. Posen, and A. Grassellino, *Phys. Rev. Appl.* **13**, 034032 (2020).
- [73] F. Yoshihara, T. Fuse, Z. Ao, S. Ashhab, K. Kakuyanagi, S. Saito, T. Aoki, K. Koshino, and K. Semba, *Phys. Rev. Lett.* **120**, 183601 (2018).
- [74] M. Hofheinz, H. Wang, M. Ansmann, R. C. Bialczak, E. Lucero, M. Neeley, A. D. O'Connell, D. Sank, J. Wenner, J. M. Martinis, and A. N. Cleland, *Nature (London)* **459**, 546 (2009).

- [75] F. Wulschner, J. Goetz, F. R. Koessel, E. Hoffmann, A. Baust, P. Eder, M. Fischer, M. Haerberlein, M. J. Schwarz, M. Pernpeintner, E. Xie, L. Zhong, C. W. Zollitsch, B. Peropadre, J.-J. G. Ripoll, E. Solano, K. G. Fedorov, E. P. Menzel, F. Deppe, A. Marx *et al.*, *EPJ Quantum Technol.* **3**, 10 (2016).
- [76] R. Dassonneville, R. Assouly, T. Peronnin, A. A. Clerk, A. Bienfait, and B. Huard, *PRX Quantum* **2**, 020323 (2021).
- [77] A. Eickbusch, V. Sivak, A. Z. Ding, S. S. Elder, S. R. Jha, J. Venkatraman, B. Royer, S. M. Girvin, R. J. Schoelkopf, and M. H. Devoret, *Nat. Phys.* **18**, 1464 (2022).
- [78] J.-K. Xie, S.-L. Ma, and F.-L. Li, *Phys. Rev. A* **101**, 042331 (2020).
- [79] Y.-Y. Lai, G.-D. Lin, J. Twamley, and H.-S. Goan, *Phys. Rev. A* **97**, 052303 (2018).
- [80] X.-K. Li, S.-L. Ma, Y.-L. Ren, J.-K. Xie, and F.-L. Li, *J. Opt. Soc. Am. B* **39**, 69 (2022).
- [81] P.-B. Li, Y. Zhou, W.-B. Gao, and F. Nori, *Phys. Rev. Lett.* **125**, 153602 (2020).
- [82] A. A. Clerk, K. W. Lehnert, P. Bertet, J. R. Petta, and Y. Nakamura, *Nat. Phys.* **16**, 257 (2020).
- [83] Z.-L. Xiang, S. Ashhab, J. Q. You, and F. Nori, *Rev. Mod. Phys.* **85**, 623 (2013).